催 化 学 报
2010 Chinese Journal of Catalysis Vol. 31 No. 2

文章编号: 0253-9837(2010)02-0163-08 DOI: 10.3724/SP.J.1088.2010.90830 研究论文: 163~170

高效自组装二氧化钛纳米管阵列光电催化降解葡萄糖的动力学和机理

刘冰川, 李金花, 周保学, 郑 青, 白 晶, 张嘉凌, 刘艳彪, 蔡伟民
上海交通大学环境科学与工程学院, 上海 200240

摘要: 研究了自组装 TiO_2 纳米管 (TNAs) 光电催化降解葡萄糖的动力学和机理. 利用薄层反应器进行耗竭反应, 研究了 TNAs 表面催化反应和溶液本体-扩散层传质有关的葡萄糖降解过程. 采用电流-时间曲线以及相应的微分曲线分析了光电化学催化降解的微观进程. 结果表明, 葡萄糖的初始浓度与降解的起始电流强度符合 Langmuir 吸附等温式 $I_{0ph}=0.00008c_0/(1+0.69274c_0)+0.00034$, 葡萄糖在 TNAs 薄膜催化剂表面的吸附为单一分子层吸附, 其光电催化降解反应符合一级反应动力学, 葡萄糖降解反应经历了三个不同的反应过程.

关键词: 自组装二氧化钛纳米管阵列; 光电化学催化反应; 葡萄糖; 薄层反应器; 反应动力学; 机理

中图分类号: O643 **文献标识码:** A

Kinetics and Mechanisms for Photoelectrochemical Degradation of Glucose on Highly Effective Self-Organized TiO_2 Nanotube Arrays

LIU Bingchuan, LI Jinhua, ZHOU Baoxue*, ZHENG Qing, BAI Jing, ZHANG Jialing, LIU Yanbiao, CAI Weimin

School of Environmental Science and Engineering, Shanghai Jiaotong University, Shanghai 200240, China

Abstract: The kinetics and mechanisms of photoelectrochemical catalytic degradation of glucose on self-organized TiO_2 nanotube arrays (TNAs) were investigated. A thin-layer cell was used to obtain an exhausted reaction condition with which an overall degradation process of glucose could be identified including surface reaction on TNAs and mass transfer from body solution to the diffuse layer. Current-time (I_{ph}-t) and the corresponding differential coefficient profiles were used to analyze the micro-processes of photoelectrochemical catalytic degradation. The initially generated photocurrents on glucose degradation versus glucose concentrations fits well with Langmuir adsorption isotherm, $I_{0ph}=0.00008c_0/(1+0.69274c_0)+0.00034$. This confirmed the adsorption of glucose on TNAs film catalyst was a single molecule layer adsorption, and the photoelectrochemical catalytic degradation reaction kinetics on TNAs surface belonged to a first-order reaction. After the initial quick reaction, three consecutive micro kinetic processes were revealed by the differential coefficient profiles (dI_{ph}/dt-t) of the glucose degradation profiles (I_{ph}-t).

Key words: self-organized titania nanotube array; photoelectrochemical catalytic reaction; glucose; thin-layer cell, kinetic; mechanism

Titanium oxide (TiO_2) has proven to be a promising catalyst for use in many aspects of environmental applications because of its high photocatalytic efficiency, nontoxicity, nonphotocorrosiveness, favorable biological and chemical inertness, and inexpensive characteristics [1]. In spite of these advantages, TiO_2 has been reported to have three non-negligible limitations [2]: (1) The high rate of electron/hole pair recombination among TiO_2 particles greatly diminished the electron-transporting efficiency; (2) Poor activation was observed when traditional TiO_2 particles are illuminated by visible light; (3) Traditional TiO_2 catalysts are generally applied through dispersion into the reaction solution, which can cause post-treatment problems.

In order to overcome these deficiencies, new TiO_2 structures such as nanorings, nanowires, nanorods, nanotubes, nanobelts, etc. were developed [3–5]. In 2001, Gong et al. [6] prepared highly ordered TiO_2 nanotube arrays (TNAs) about 500 nm in length by potentiostatic anodization of

Received date: 29 August 2009.
***Corresponding author.** Tel/Fax: +86-21-54747351; E-mail: zhoubaoxue@sjtu.edu.cn
Foundation item: Supported by the National High Technology Research and Development Program of China (863 Program, 2009AA063003), the Science and Technology Commission of Shanghai Municipality (08JC1411300, 0952NM01800), and the National Natural Science Foundation of China (20677039).
English edition available online at ScienceDirect (http://www.sciencedirect.com/science/journal/18722067).

titanium in HF aqueous solution. The nanotubular microstructures were perpendicular to the electrically conductive Ti substrates, forming a Schottky-type contact naturally and providing a unidirectional electric channel for the transport of photo-generated electrons [7]. Hence, as an electrode in photoelectrochemical catalysis, TNAs have shown good charge transport properties and elevated photoelectrical and electrochemical performance [8,9]. For example, TNAs-based photoanodes have been reported as an excellent photoelectrocatalyst for the degradation of various organic pollutants [10]. Titania materials have also been used to improve the photosplitting of water [11] and for dye-sensitized solar cells [12,8]. In our recent work [13,14], a TNAs-based chemical oxygen demand (COD) sensor can achieve rapid and accurate COD determination of wastewater.

Photoelectrochemical catalysis oxidation of organic compounds is multiphase reactions, involving gas-solid and liquid-solid inter-phase and interfacial reactions. Generally, the degradation involves three major processes, diffusion, adsorption, and interfacial reactions. In a traditional bulk reactor, the reactant is transferred from the body solution to the surface of the TNAs. The exterior mass transfer influenced the overall degradation because of the relatively large body solution and long diffusion channel. This limits the investigation of interfacial reaction mechanism on the TNAs. However, when a thin-layer reactor with a thin reaction volume was adopted in the reaction system [13,14], the adsorption characteristics of different organic compounds and their interactions with the catalyst can be studied. The thin-layer cell with a small solution volume and a short diffusion channel can simplify the kinetic study of the degradation processes, and a detailed investigation of an interested kinetic process can be investigated without the influence of bulk solution effects. Moreover, it can help to obtain information on the maximum catalytic capability of a heterogeneous reaction system, to identify the limiting steps, and to optimize the catalytic conditions of TNAs. Hence, the investigation of the degradation characteristics of organic compounds in the thin-layer reactor is crucial for understanding the kinetics and mechanism of the surface reaction on TNAs catalyst.

In this study, glucose was chosen as a model compound to investigate the kinetics and mechanisms of photoelectrochemical catalytic degradation on self-organized TNAs under the conditions of a thin-layer cell. The influences of concentration and illumination intensity on kinetics and mechanisms of photoelectrochemical catalytic degradation were also discussed.

1 Experimental

1.1 Preparation and characterization of TNAs

Titanium sheet (0.1 mm thick, 99.9% purity) was anodized at 20 V for 0.5 h in a 0.5% HF acid electrolyte at 25 °C [6,15]. Platinum was applied as the counter electrode. The counter electrode Pt had the same size as the titanium sheet, and both were parallel with each other in the electrolyte during the anodization. After anodization, the formed nanotube film sample was annealed at 500 °C for 3 h at a heating and cooling rate of 1 °C/min to crystallize into anatase crystalline form. The morphology of the annealed TNAs was characterized by scanning electron microscopy (SEM) using a Philips Sirion200 microscope. The crystal phase of the TNAs was characterized by X-ray diffraction (XRD) using a Bruker AXS-8 Advance diffractometer.

1.2 Assembly of the thin-layer cell photoelectrocatalytic reactor

The thin-layer reactor included six main components: a cell body, a TNAs anode, a Pt cathode, a saturated AgCl/Ag reference electrode, a flow inlet, and a flow outlet. Two Teflon boards were compressed together to form a space (0.1 mm thickness) along with screw bolts and nuts. The front Teflon board was also embedded with a quartz window (0.785 cm^2), which was used to admit illumination. Silicon gel was used to seal all interstices in the thin-layer cell to keep the reactor airtight. The thin-layer cell reactor was connected to an electrochemical workstation and a computer to process the data.

1.3 Photoelectrochemical experiments

Current-time profiles (*I*-*t*) and current-potential profiles (*I*-*V*) were measured using an electrochemical workstation (CH Instruments, USA, CHI660C) connected to a computer. Illuminations were carried out using a 4 W UV lamp (254 nm, GE, Japan, G4T5) and the light intensity was measured by an UV-irradiance meter (Beijing Normal University, China, UV-B). Sodium dihydrogen phosphate (AR) and D-(+)-glucose anhydrous (AR) were all provided by Sinopharm Chemical Reagent Co., Ltd. All solutions were prepared using high-purity deionized water. All experiments were carried out at room temperature.

2 Results and discussion

2.1 SEM and XRD results

Figure 1 shows the morphology of the annealed TNAs film. It can be observed that the nanotubes are highly ordered and well aligned. Observations from the cross-section reveal that the nanotubes are ~300 nm in length and tightly combined with the barrier layer. In comparison with the

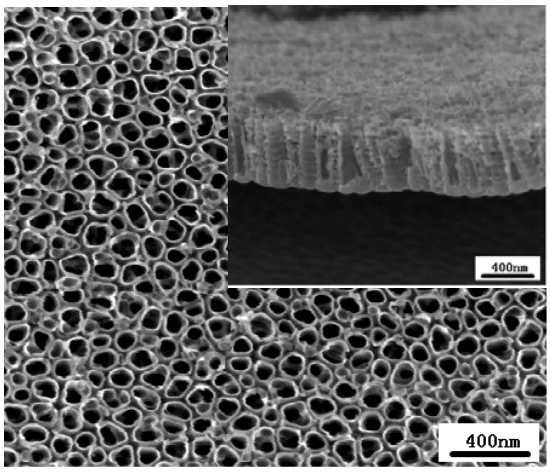

Fig. 1. SEM images of the top view and cross-section (inset) of TiO_2 nanotube arrays (TNAs) formed at 20 V for 0.5 h in a 0.5% HF acid electrolyte after annealing.

long TNAs, the current data show that the TNAs are short, quite robust, and ordered. Therefore, they can offer higher activity and stability in the long-term operation for the degradation of organic compounds [7].

The XRD patterns of the as-annealed TNAs electrode are shown in Fig. 2, which indicated that the annealing process directly transformed the as-formed TNAs film from amorphous to anatase phase, as confirmed by the 25.4° (101), 38.1° (004), and 48.2° (200) characteristic peaks.

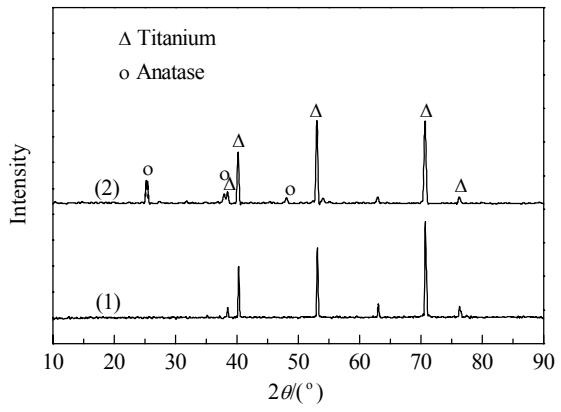

Fig. 2. XRD patterns of the TNAs. (1) As-prepared; (2) After calcination at 500 °C.

2.2 Selection of appropriate potential bias

For a thin-layer cell, a high-concentration electrolyte was applied to avoid the IR drop and the deformation of current-potential responses created by the resistance from the solution between the working and reference electrode. A 2.0 mol/L NaH_2PO_4 was chosen as electrolyte because of its unique characteristics [16]. In order to focus on the investigation of the kinetic process of interest, an appropriate potential bias is needed to affect the kinetics of a photoelectrolysis process by facilitating the process of electron transport across the semiconductor film. A continuous cyclic voltammogram (I_{ph}-V) scan was conducted to confirm the effectiveness of the potential bias.

Figure 3 shows three typical continuous cyclic voltammograms of a self-organized TNAs electrode film using 2.0 mol/L NaH_2PO_4 supporting electrolyte in the thin-layer cell under different UV illumination intensity. The potential was ramped from 0 to 4.0 V. The I_{ph}-V profile (Fig. 3(a)) shows three replicates under illumination intensity of 2.46 mW/cm^2. The excellent reproducibility of the I_{ph}-V profiles suggested that this photoelectrochemical methodology in a thin-layer cell can show good reproducibility in photoelectrochemical catalytic performance under UV illuminations. The photocurrent platforms were all acquired within +1.0 and +3.0 V, which reveal a wide electrochemical window for TNAs. Therefore, when the potential bias was chosen within +1.0 and +3.0 V, a photocurrent response can be obtained, which represents the rate of electron captured at the interface without the influence from the electron transport across the TNA film. In addition, Fig. 3(b) shows that the photocurrents increased with illumination intensities (the I_{ph}-V curves were acquired under illumination intensities of 2.46, 1.29, and 0.78 mW/cm^2, respectively). Following this trend, a +2.2 V potential bias was chosen for the

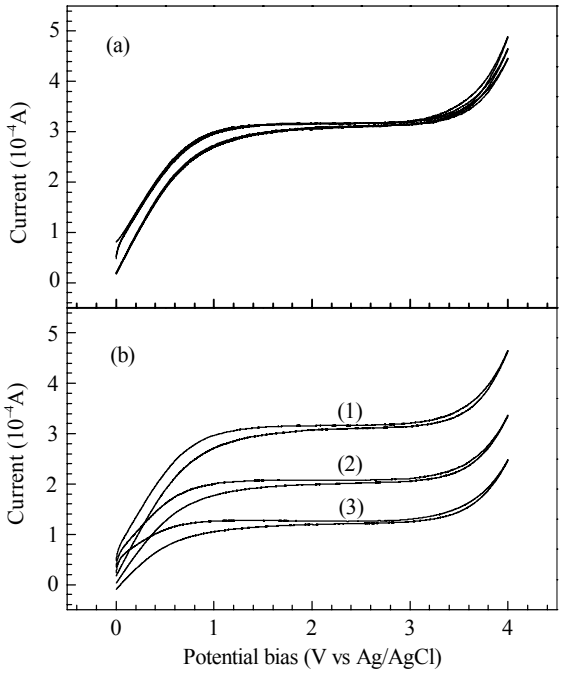

Fig. 3. (a) Three continuous cyclic voltammograms of a self-organized TNA electrode film in 2.0 mol/L NaH_2PO_4 electrolyte under 2.46 mW/cm^2 UV illumination intensity. (b) Continuous cyclic voltammograms under three different UV illumination intensities. (1) 2.46 mW/cm^2; (2) 1.29 mW/cm^2; (3) 0.78 mW/cm^2.

experiments in this study.

2.3 Photoelectrochemical degradation of glucose

Under 3.05 mW/cm^2 UV illumination intensities, several dynamic I_{ph}-V voltammograms of glucose degradation were scanned. In the thin-layer cell reactor, real time data on photoelectrochemical catalysis degradation efficiency were acquired under different concentrations and 2.0 mol/L NaH_2PO_4 electrolyte. On account of the high rate of degradation at the beginning, a 1 V/s scanning rate was applied. As shown in Fig. 4, all I_{ph}-V profiles increased within the potential bias of 0.0–1.5 V followed by a slight decrease within 1.3 and 3 V due to the rapid photoelectrochemical degradation. After that, a precipitous increase in photocurrent was observed after +3.0 V. As the potential began to surpass the oxidizing potential of water, it triggers the electron transfer of the oxygen and explains the reason for the increase in photocurrent response. Moreover, the value of photocurrents was observed to increase along with the corresponding glucose concentrations.

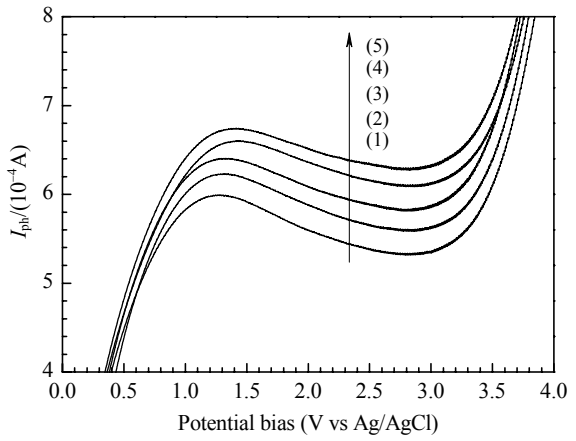

Fig. 4. Voltammograms using the TNA film electrode in solutions of 2.0 mol/L NaH_2PO_4 containing different concentrations of glucose under 3.05 mW/cm^2 UV illumination. (1) 0.25 mmol/L; (2) 0.5 mmol/L; (3) 1 mmol/L; (4) 2 mmol/L; (5) 3 mmol/L.

2.4 Typical photocurrent-time profile of glucose

Figure 5 shows a typical photocurrent response of a blank solution of 2.0 mol/L NaH_2PO_4 (Fig. 5(2)) and photocurrent response of a 2.0 mol/L NaH_2PO_4 solution containing 1.2 mmol/L glucose in a thin-cell reactor (Fig. 5 (1)). Both solutions were operated under the same illumination intensity. The even photocurrent observed for the blank solution (Fig. 5(2)) originated from the stable oxidation of water. The photocurrent response originated from two ways: water oxidation and glucose mineralization. In the initial stage (about less than 1 s), a transient photocurrent spike was

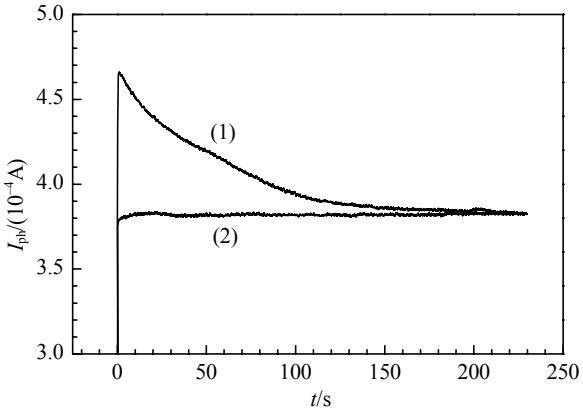

Fig. 5. Typical photocurrent response of 2.0 mol/L NaH_2PO_4 blank solution (1) and 2.0 mol/L NaH_2PO_4 solution containing 1.2 mmol/L glucose (2) under 2.63 mW/cm^2 UV illumination using the thin-cell reactor based on a TNA film catalyst.

observed because of the degradation of the glucose molecules originally accumulated on the TNA surface (Fig. 5(1)). When the photocurrent reached the peak (I_{0ph}), it began to decrease quickly owing to the glucose mineralization and a relatively large ratio between electrode area and solution volume. After the exhaustion of the glucose in the thin-layer reactor, the photocurrent finally reached a stable value, which implied that the glucose in the thin-layer cell reactor was completely mineralized. Compared with the bulk reactor, the reaction in the thin-layer cell was exhaustive. The total number of electrons generated due to the glucose oxidization can be expressed as $Q_{net} = Q_{total} - Q_{background}$, where Q_{net} is the theoretical net charge from the overall glucose degradation, Q_{total} is the theoretical net charge from the oxidation of glucose and water, and $Q_{background}$ is the theoretical net charge from the oxidation of water.

The stoichiometric oxidation of glucose can be represented as $C_6H_{12}O_6 + 6H_2O \rightarrow 6CO_2 + 24H^+ + 24e^-$. The mineralization of 1 mol of glucose requires 24 mol electrons. Thus, the Faraday's law can be written as $Q_{net} = 24FVc_0 = kc_0Q_{net}$, where V is the volume of the thin-layer cell, F is the Faraday constant, and c_0 is the initial concentration of glucose. Consequently, the quantum of glucose can be converted equivalently according to the amount of the net charge.

Based on the measurement of the total number of photoelectrons generated from the photocatalytic oxidation of organics, the photoelectrochemical method can easily quantify the degree of the degradation according to Faraday's law, assuming that we can ignore the complicated interim reactions in the traditional photoelectrochemical degradation method. The rate of electron capturing (i.e., the value of the photocurrent) can directly describe the photocatalytic degradation efficiency.

2.5 Kinetics and mechanisms of photoelectrochemical catalytic degradation

2.5.1 Influences of glucose concentration on initial photocurrent responding

Figure 6 shows different initial glucose concentrations and their corresponding peaks of I_{0ph}. c_0 represents the initial glucose concentrations, and the peak photocurrent I_{0ph} was obtained from each degradation profile (Fig. 5). As shown in Fig. 6, the maximum photocurrents increased with corresponding increase in initial concentrations of glucose. At low concentration of glucose, I_{0ph} was proportional to the initial glucose concentration, which resulted in the photohole capture process in the glucose mineralization. However, as the glucose concentration increased to the extent where the photohole generation (light intensity-dependent) was the limiting step, the increasing trends of I_{0ph} began to alleviate.

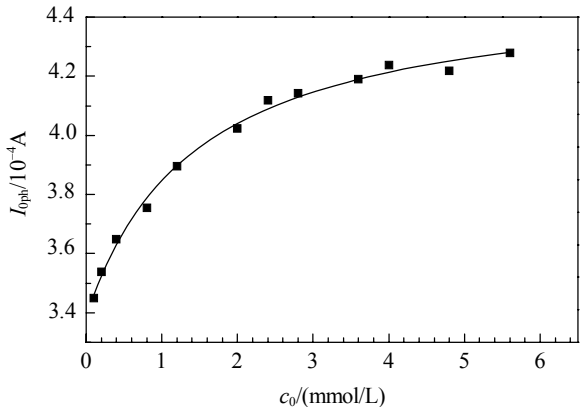

Fig. 6. A plot of saturated photocurrents (I_{0ph}) against concentrations of glucose solution (c_0) for degradation of glucose in 2.0 mol/L NaH_2PO_4 electrolyte under 2.50 mW/cm^2 UV illumination.

Computer simulation reveals that the I_{0ph}-c_0 profile is fitted to Eq. (1) written as

$$I_{0ph} = P_1c_0/(1 + P_2c_0) + P_3 \quad (1)$$

where P_1, P_2, and P_3 are three parameters equal to 0.00008, 0.69274, and 0.00034, respectively. P_1, P_2, and P_3 are 9.0781E–6, 0.09089, and 2.3563E–6, respectively, within the limits of experimental error. Computer simulation showed that the determination coefficient of the fitting profile is 0.99503, which showed a considerable accordance with the I_{0ph}-c_0 profile. Thus, Eq. (1) can be written as

$$I_{0ph} = 0.00008c_0/(1 + 0.69274c_0) + 0.00034 \quad (2)$$

P_3 = 0.00034 is the intercept of the fitted profile extension line with the ordinate axis, which means 0.00034 A is the current value generated by merely the oxidation of water.

Because the initial degradation rate R was responding to the value of I_{0ph}, it could be written as

$$R = k_1I_{0ph} = 0.00008c_0k_1/(1 + 0.69274c_0) + 0.00034k_1 \quad (3)$$

For a single reactant (such as glucose) degradation in a thin-layer cell, the internal mass transfer on the surface of TNA film could be ignored as mentioned above. At the same time, the adsorption and desorption processes of glucose were very fast, which rendered the reaction to be balanced at each step. Therefore, the catalyst-solution interfacial reaction rate could be written as

$$R = k'\theta_A{}^n [h^+]^m + B \quad (4)$$

where k' is the reaction constant, θ_A is the coverage of glucose on TNA film, $[h^+]$ is the surface concentration of photoholes on TNA film, and B is the rate of water oxidation. Because $[h^+]$ possesses a large quantity and is merely determined by the property of TNAs, it can be considered as a constant in this reaction. Therefore Eq. (4) can also be written as

$$R = k\theta_A{}^n + B \quad (5)$$

According to Eqs. (3) and (5), θ_A was interrelated to $0.00008c_0/(1+0.69274c_0)$, which can be written as

$$\theta_A = 0.00008c_0k_2/(1 + 0.69274c_0) \quad (6)$$

Eq. (6) was also observed to be similar to the Langmuir-Hinshelwood adsorption equation regardless of interception. The Langmuir-Hinshelwood adsorption equation can be written as

$$\theta_A = a_AP_A/(1 + a_AP_A) \quad (7)$$

where P_A and a_A are the equilibrium pressure and the adsorption equilibrium constant of glucose on TNAs, respectively. P_A was decided by the initial concentration of glucose in body solution and could be written as

$$P_A = k''c_0 \quad (8)$$

Substituting Eq. (8) into Eq. (7) gives

$$\theta_A = k''a_Ac_0/(1 + a_Ak''c_0) \quad (9)$$

Comparing Eq. (5) with Eq. (3) gives

$$R = k_1I_{0ph} = 0.00008c_0k_1/(1+ 0.69274c_0)+0.00034k_1$$
$$= k(k''a_Ac_0/(1 + a_Ak''c_0))^n + B \quad (10)$$

Eq. (10) shows that the profile of c_0 vs I_{0ph} matched well with Langmuir adsorption isotherm. In addition, comparing the left and the right part of Eq. (10) gives n = 1. Hence Eq. (5) could be written as

$$R = k\theta_A+B \quad (11)$$

which means that the adsorption of glucose on the surface of the TNA catalyst can be explained as a single molecule layer adsorption and the reaction on catalyst belongs to first-order reaction. In summary, the initial reaction rate could be written as

$$R = 0.00008c_0k_1/(1 + 0.69274c_0) + 0.00034k_1 \quad (12)$$

2.5.2 Influences of illumination intensity on photoelectrochemical catalytic degradation

Figure 7 shows the photocurrent-time profiles of the photoelectrochemical degradation of glucose with the iden-

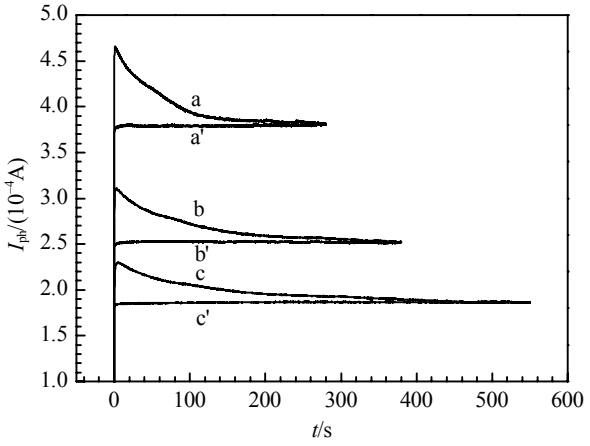

Fig. 7. Photocurrent-time profiles of glucose degradation under 2.6, 1.3, and 0.7 mW/cm^2 UV illumination intensities, respectively. a, b, and c are photocurrent responds of 1.2 mmol/L glucose plus 2.0 mol/L NaH_2PO_4 electrolyte. a′, b′, and c′ are photocurrent responds of 2.0 mol/L NaH_2PO_4 electrolyte.

tical concentration under strong, moderate, and weak UV illumination intensities, respectively. The profile shapes are similar to each other, and the glucose was finally mineralized completely. However, the values of photocurrents with different illumination intensities and the time for exhausted photoelectrochemical degradation were distinctively different. Particularly, the time taken for exhausted degradation from the strong illumination to weak illumination were 230, 350, and 500 s, respectively, which means the increased illumination intensity can reduce the degradation time and enhance photoelectrochemical catalytic efficiency.

Further calculation shows that the values of Q_{net} on a/a′, b/b′, and c/c′ are 0.005530, 0.005285, and 0.005550 Coulomb, respectively. This indicates that the glucose degradations under different illumination intensities can generate similar Q_{net}, showing an excellent reappearance.

2.5.3 Influences of glucose concentration on kinetic processes of photoelectrochemical catalytic degradation

Figure 8(a) shows the I_{ph}-t and dI_{ph}/dt-t profiles of the photoelectrochemical degradation of glucose with different concentrations under 2.50 mW/cm^2 illumination intensity. Generally, the degradation profiles of glucose with different concentrations reveal similar variation trends (Fig. 8(1)). However, there are still differences among the differential coefficient profiles, indicating the disparities in the kinetic processes of glucose degradation at different concentrations.

Figure 9 shows the micro-mechanism of mass transfer of the degradation reaction. In a stable state of glucose solution, a diffuse layer exists between the TNA surface and the body solution. Stable adsorption of glucose on catalyst was basically divided into three consecutive steps, including glucose molecule transfer from the body solution to the diffuse layer, from the diffuse layer to the TNA surface, and the glucose molecule adsorption on the TNA surface. In practice, the diffusion of glucose molecules from body solution to the diffuse layer was caused by molecular pressure on the interface of the two parts. The glucose molecules were then transferred to the surface of the catalyst from the diffuse layer and finally accumulated on TNA. In general, the rate of glucose transfer from body solution to the diffuse layer is slower than that from the diffuse layer to the TNA surface under a stable solution condition in the thin-layer cell. This was expected to make the former process a limiting step for the overall reaction.

The comparison of I_{ph}-t profiles of glucose degradation with different concentrations (Fig. 8(1)) shows that the reaction rates increased with the increased initial concentra-

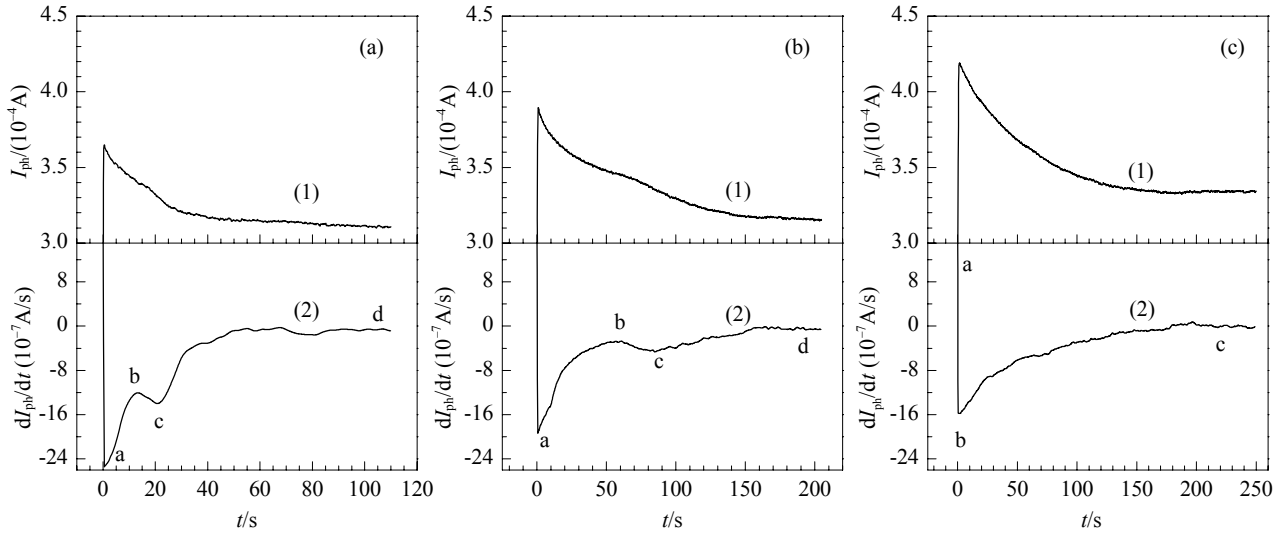

Fig. 8. I_{ph}-t (1) and dI_{ph}/dt-t (2) profiles of glucose plus 2.0 mol/L NaH_2PO_4 degradation under 2.50 mW/cm^2 UV illumination. Glucose concentration: (a) 0.4 mmol/L; (b) 1.2 mmol/L; (c) 3.6 mmol/L.

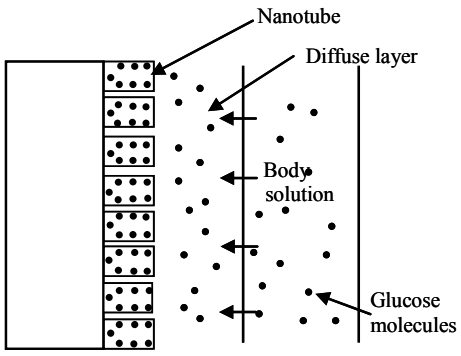

Fig. 9. Schematic depiction of the glucose transfer through the interface of the body solution and the diffuse layer.

tions, but the time for complete degradation was extended as the concentration increased. Transient photocurrent spikes in all glucose degradation I_{ph}-t profiles were observed instantaneously in the initial stage (less than 1 s), indicating that the glucose initially accumulated on the TNA film was oxidized quickly. The amount of the initially accumulated glucose was decided by the solution-TNAs interface adsorption equilibrium. Then they all reached the complete mineralization. The comparison also shows that there were differences in the processes of glucose degradation. For example, at the low concentration (0.4 mmol/L, Fig. 8(a-1)), after a rapid increase in I_{ph}, dI_{ph}/dt experienced three major processes: a rapid increase, a decrease, and a re-increase that leveled off to zero, and the corresponding sections in its differential coefficient profile were in the section about 1–14, 14–22, and 22–100 s, respectively (Fig. 8(a-2), a–b, b–c, and c–d).

The above kinetic processes can be explained as follows. The quick oxidation of glucose initially accumulated on the TNA film surface caused a sudden drop in glucose coverage rate on the TNA film surface. Thus the I_{ph} kept on decreasing afterwards. At the same time, glucose molecules in the diffuse layer began to replenish the oxidized glucose molecules on TNA surface, which caused a decline in glucose concentration in the diffuse layer. However, the glucose molecules in the body solution could not sufficiently supplement the rapid consumption of glucose in the diffuse layer. This part was manifested as a slow drop in I_{ph}, and the corresponding dI_{ph}/dt-t profile has shown an increase in the section of about 1–14 s (Fig. 8(a-2), a–b). As the reaction progress, the glucose molecules kept on transferring from the body solution to the diffuse layer, and the glucose concentration in the diffuse layer increased. Consequently, the amount of glucose molecules transferring to the TNA film surface began to increase. When the rate of glucose molecule transferring from diffuse layer to TNA surface exceeded the reaction rate on TNA surface, the glucose absorbents coverage began to increase and so did the degradation rate. Therefore, the corresponding dI_{ph}/dt-t profile has shown a decrease in the section of about 14–22 s (Fig. 8(a-2), b–c). After the section of 14–22 s, the concentration difference of glucose molecules between the body solution and diffuse layer began to diminish, and the glucose concentration in the body solution was gradually decreased. The diffusion driving force of glucose molecule between the body solution and the diffuse layer became weak, and the coverage rate of glucose on TNA film showed an accelerated decline tendency, which caused a gradual retard in the decrease of I_{ph}. This process was shown in the dI_{ph}/dt-t profile in the section of about 22–40 s with a gradual increase (Fig. 8(a-2), c–d). When all the glucose molecules in the body solution, in the diffuse layer, and on the surface of TNA film were removed completely, the value of I_{ph} began to be stable and the dI_{ph}/dt-t profile leveled off to zero (Fig. 8(a-2), c–d).

From the above analysis, it can be concluded that the molecule diffusion process from the body solution to the diffuse layer is a controlling step of the overall catalyst reaction processes. The molecule diffusion process from the diffuse layer to the surface of TNA film also strongly affects the degradation rate. The surface reaction of glucose molecules on catalyst surface is a fast reaction step.

Fig. 8(b-2) also reveals three major processes of glucose degradation with moderate concentration (Fig. 8(b-2), a–b, b–c, and c–d, about 1–55, 55–75, and 75–200 s, respectively). However, because of the higher glucose concentration in the body solution, the diffusion driving force of glucose molecules between the body solution and the diffuse layer increased, which caused a higher glucose concentration in the diffuse layer and a thicker diffuse layer (because the solution in the thin-layer cell was not agitated, the diffuse layer can change). Compared with Fig. 8(a-2), the first increasing section of dI_{ph}/dt-t profile (Fig. 8(b-2), a–b, about 1–55 s) went through a relatively long period, and the second section (at about 55–75 s, b–c) was postponed.

Fig. 8(c-2) shows that the glucose degradation with high concentration did not experience the anticipated three main processes observed in those cases with low and moderate concentrations, and only an increase in dI_{ph}/dt was observed throughout the entire degradation process. This can be attributed to an even higher glucose concentration in the diffuse layer and an even thicker diffuse layer that caused a more powerful diffusion driving force of glucose molecules between the body solution and the diffuse layer.

3 Conclusions

The kinetics and reaction mechanism of photoelectrochemical degradation of glucose on self-organized TiO_2

nanotube arrays (TNAs) were studied. The TNAs were highly efficient in photoelectrocatalysis of glucose degradation and the catalytic efficiency increased along with illumination intensities. The adsorption of glucose on TNA catalyst was a single-layer adsorption, and glucose molecule coverage on TNA surface followed the relation $\theta_A = 0.00008c_0k_2/(1+0.69274c_0)$, indicating that the adsorption followed Langmuir adsorption isotherm. In this study we identified two steps: (1) An overall exhaustion reaction (a control step) where glucose molecules diffuse from the body solution to the diffuse layer; (2) A fastest step during which the catalytic reaction of glucose molecules is achieved on TNA surface. Three distinctive micro-kinetic processes were demonstrated in the photoelectrochemical degradation processes after the initial quick reaction. The corresponding three dI_{0ph}/dt processes include a rapid increase, a decrease, and a re-increase leveling off to zero. As glucose concentrations increase, the boundaries of the three micro-processes became unobvious. The results show that the application of the thin-layer cell reactor to investigate the photoelectrocatalytic degradation processes on the TNA catalyst can help to clarify the organic degradation kinetics and mechanisms.

References

1 Fujishima A, Honda K. *Nature*, 1972, **238**: 37
2 Park J H, Kim S, Bard A J. *NanoLett*, 2006, **6**: 24
3 Beranek R, Kisch H. *Electrochem Commun*, 2007, **9**: 761
4 Wang Y M, Du G J, Liu H, Liu D, Qin S B, Wang N, Hu C G, Tao X T, Jiao J, Wang J Y, Wang Z L. *Adv Funct Mater*, 2008, **18**: 1131
5 O'Regan B, Gratzel M. *Nature*, 1991, **353**: 737
6 Gong D W, Grimes C A, Varghese O K, Chen Z, Hu W C, Dickey E C. *J Mater Res*, 2001, **16**: 3331
7 Liu Zh Y, Zhang X T, Nishimoto S, Jin M, Tryk D A, Murakami T, Fujishima A. *J Phys Chem C*, 2008, **112**: 253
8 Mor G K, Varghese O K, Paulose M, Shankar K, Grimes C A. *Solar Energy Mater Solar Cells*, 2006, **90**: 2011
9 Grimes C A. *J Mater Chem*, 2007, **17**: 1451
10 Quan X, Yang Sh G, Ruan X L, Zhao H M. *Environ Sci Technol*, 2005, **39**: 3770
11 Paulose M, Shankar K, Yoriya S, Prakasam H E, Varghese O K, Mor G K, Latempa T A, Fitzgerald A, Grimes C A. *J Phys Chem B*, 2006, **110**: 16179
12 Liu Y B, Zhou B X, Xiong B T, Bai J, Li L H. *Chin Sci Bull*, 2007, **52**: 1585
13 Zheng Q, Zhou B X, Bai J, Li L H, Jin Zh J, Zhang J L, Li J H, Liu Y B, Cai W M, Zhu X Y. *Adv Mater*, 2008, **20**: 1044
14 Zhang J L, Zhou B X, Zheng Q, Bai J, Li J H, Liu Y B, Cai W M. *Water Res*, 2009, **43**: 1986
15 Bai J, Zhou B X, Li L H, Liu Y B, Zheng Q, Shao J H, Zhu X Y, Cai W M, Liao J Sh, Zou L X. *J Mater Sci*, 2008, **43**: 1880
16 Jin Z J, Li L H, Zheng Q, Bai J, Zhou B X, Cai W M. *Environ Protect Chem Ind*, 2006, **26**: 443